Irradiation resistance of thermo-optical properties of zirconium diboride by 3 MeV electrons

Rønning, K.D.; Tang, Y.

DOI
10.3389/frspt.2024.1355258

Publication date
2024

Document Version
Final published version

Published in
Frontiers in Space Technologies

frontiers | Frontiers in Space Technologies

TYPE Original Research
PUBLISHED 21 March 2024
DOI 10.3389/frspt.2024.1355258

OPEN ACCESS

EDITED BY
Antonio Mattia Grande,
Polytechnic University of Milan, Italy

REVIEWED BY
Ning Li,
China Academy of Engineering Physics, China
Kaustubh Bawane,
Idaho National Laboratory (DOE), United States

*CORRESPONDENCE
Yinglu Tang,
Y.Tang-5@tudelft.nl

RECEIVED 13 December 2023
ACCEPTED 29 February 2024
PUBLISHED 21 March 2024

CITATION
Rønning D and Tang Y (2024), Irradiation resistance of thermo-optical properties of zirconium diboride by 3 MeV electrons . *Front. Space Technol.* 5:1355258. doi: 10.3389/frspt.2024.1355258

Irradiation resistance of thermo-optical properties of zirconium diboride by 3 MeV electrons

Daniel Rønning and Yinglu Tang*

Aerospace Engineering Faculty, Delft University of Technology, Delft, Netherlands

Due to good thermal conductivity and thermal shock resistance, ultra-high temperature ceramics such as zirconium diboride (ZrB_2) have been investigated as promising materials to be used in reusable thermal protection systems TPSs are vital to the heat balance of a spacecraft during atmospheric reentry and subsequent operation in space. Hence, the thermal and optical properties are especially critical for such applications. Meanwhile, radiation exposure in space can pose risks of degrading such material properties, especially over a prolonged mission duration. The interaction of electron radiation-which can be found in the outer Van Allen belt, with ZrB_2 has not been studied previously and was chosen as the main scope of this study. An electron source of 3 MeV with different radiation exposure time was used. The response of thermo-optical properties of ZrB_2 to increasing electron radiation fluences was investigated. ZrB_2 samples were made through spark plasma sintering into sintered pellets and then exposed to 3 MeV electron irradiation. These ZrB_2 samples were characterized by their microstructure, thermal conductivity, coefficient of thermal expansion (CTE), emittance, absorptivity, and surface roughness before and after irradiation. It was found that ZrB_2's thermo-optical properties showed high radiation resistance at these fluences, and no apparent microstructural change was observed after irradiation. However, the irradiated samples had, on average, a 29% lower surface roughness than the unirradiated samples, possibly originating from electron sputtering.

KEYWORDS

zirconium diboride, electron irradiation, thermal protection systems, thermal properties, optical properties

1 Introduction

Zirconium diboride has been investigated for use in nuclear and aerospace applications since the 1950s. ZrB_2 has a hexagonal crystal structure, layered with alternating planes of closed packed hexagonal Zr and B. Zr atoms are situated directly above/below 6-membered rings in the adjacent Boron planes. ZrB_2 is a metal diboride MB_2 ceramic which is similar in crystal structure as the other variations such as HfB_2. These borides are considered as superior alternatives compared to carbides and nitrides for specific high-temperature applications, as they have excellent mechanical properties, thermal properties, and oxidation resistance (Guria et al., 2021).

One of the most common uses of these diboride ceramics in space is in refractory reentry heat shields or thermal protection coating. Due to its excellent thermomechanical qualities,

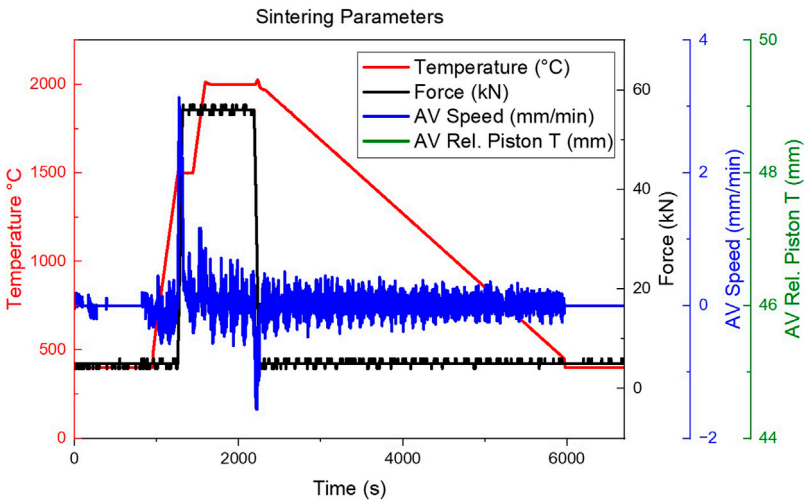

FIGURE 1
SPS Temperature, force, piston speed and translation.

including a high melting temperature, high thermal conductivity and relatively good thermal shock resistance compared to other ceramics, it has been studied for its possible use as thermal protection system material in hypersonic flight and reentry spacecraft. There is potential for diboride UHTC heat shields to increase the reusability of reentry spacecraft, in contrast to ablative heat shields which need to be continuously replaced, such as carbon-carbon composites. Compared to other high temperature application materials such as C/SiC and SiC/SiC composites, UHTC borides display not only high temperature capability but also high thermal conductivity (Sengupta and Manna, 2019). However, zirconium diboride has not been widely used in space yet compared to other ceramics such as silicon carbide. This is partly due to the material's large density and sintering/manufacturing challenge due to its high melting point, in addition to its small fracture toughness which makes diboride-based ceramic matrix composites necessary.

The primary heat sources for a reentry vehicle are convection between hot surrounding gas and the vehicle and radiative heating from the shock layer on the body. Both heat sources depend on the velocity and leading-edge radius of the spacecraft and the density of the medium. On the other hand, radiative cooling depends on the thermal emittance of the surface, Stefan-Boltzmann constant, and the temperature of the body, T. The temperature on the spacecraft's surface can be calculated by balancing the outward radiative cooling with radiative and convective heating (Johnson et al., 2014). While the radiative heating and cooling is largely influenced by optical properties, the amount of heat transported to the spacecraft and its components is related to the thermal conductivity of the heat shield. Therefore, these properties are fundamental to the viability of ZrB_2 as a heat shield material, especially when they are exposed to long term irradiation in space missions (Christa et al., 2002).

In metals and ceramics, irradiation reduces thermal and electrical conductivity. This is because incoming radiation creates atom displacements. These defects render the crystal structure more disordered, and as a result, slow down thermal and electric transport (EPA, 2020). Weisensee, Feser, and Cahill (Weisensee et al., 2013) investigated the effect of increasing Argon radiation doses on the thermal conductivity of a thin film of uranium oxide. This was done for samples at irradiation fluences of 0.05×10^{15}, 0.7×10^{15} and 10×10^{15} $Ar^{+}cm^{-2}$, where the thermal conductivity was measured through time-domain thermoreflectance. The thermal conductivity of unirradiated UO_2 was 10.2 Wm^{-1} K^{-1} at 323 K and scaled with temperature like 1/T. It was observed that the conductivity decreased to less than 4 Wm^{-1} K^{-1} upon irradiation doses $>0.7 \times 10^{15}$ Ar^{+} cm^{-2} and the scattering strength of irradiation induced point defects was reported. Higher irradiation levels did not cause a further decrease in conductivity.

Garrison et al. (Garrison et al., 2018a) investigated the damage to ZrB_2 by 30 keV He irradiation as plasma-facing materials in fusion reactors. This was done at temperatures between 920–1120 K and two different Helium fluences of 8.41×10^{21} He/m^2 and 5×10^{22} He/m^2 with six samples. Surface morphology changes, such as ripples and pores, were observable at higher irradiation fluences. It was also found that the surface of the ZrB_2 samples changed from a matte grey to blue and brown in the irradiated areas. The intensity of the color change was more significant at higher fluences. There was also a mass loss from ion implantation and sputtering mechanisms, but no apparent relationship between the mass loss and the irradiation fluence or temperature was observed.

With an increasing need for space exploration and reusability concerns, there is a clear need for research into the effects of long term radiation on spacecraft materials. Despite the fact that particle sources, such as helium particles, protons, or Argon can cause more damage and simulate closer radiation condition in Solar Particle Events (SPE) and Galactic Cosmic Rays (GCR), this study's main scope is to investigate the electron irradiation resistance of thermal and optical properties of bulk ZrB_2 as a potential TPS material in space applications. The radiation type in this study was chosen to be electron radiation to represent that in the Van Allen belt's outer rim. This is especially relevant for geostationary satellite deployment, Moon missions, or deeper space missions (Christa et al., 2002). In the Van Allen belt's

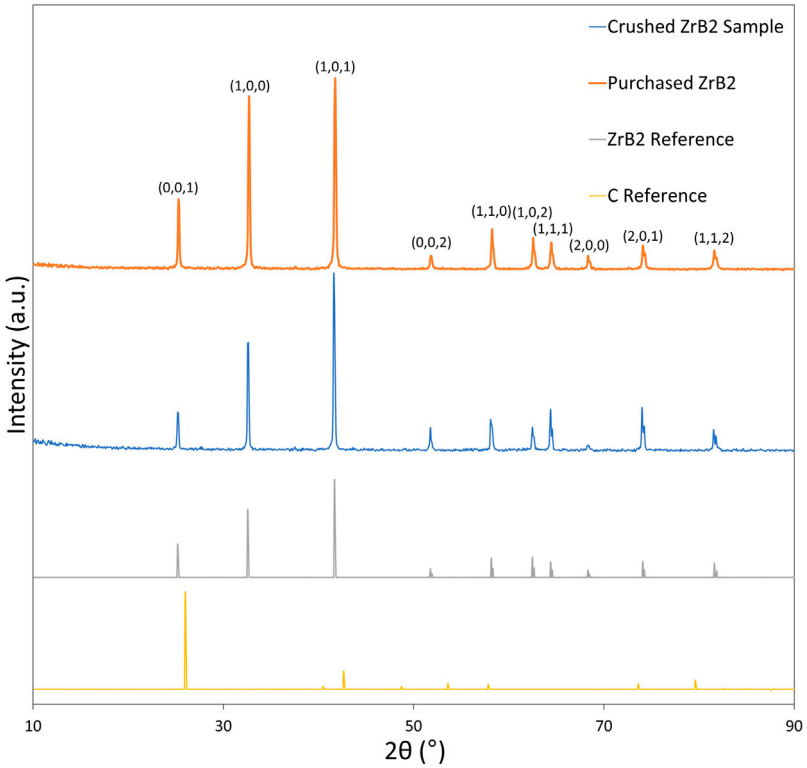

FIGURE 2
XRD-analysis of crushed ZrB_2 powder from sps-ed pellet, raw ZrB_2 powder, ZrB_2 reference and graphite reference data.

TABLE 1 Van de Graaf fluence, flux and exposure time of ZrB_2 samples.

Flux ($e^-cm^{-2}s^{-1}$)	Fluence (e^-cm^{-2})	Exposure time (s)
5.55E+11	1576.9E+11	283.54
6.76E+11	3153.8E+11	466.00
8.35E+11	15769.4E+11	1886.97

TABLE 2 Lattice parameters of sintered ZrB2 samples from XRD measurements (hand calculated) and that was calculated by Vesta software.

Lattice parameter c (Å)		Lattice parameter a (Å)	
Calculated	Vesta	Calculated	Vesta
3.524 ± 0.004	3.531	3.166 ± 0.001	3.169

outer rim, electrons have energies ranging from 0.1 to 10 MeV, whilst the electron source employed in this study is a 3 MeV electron from a system called Van de Graaf at the reactor institute of TU Delft. While electron irradiation with energy range 1–3 MeV has been used to determine space irradiation degradation of thin film solar cells, such as $Cu(In,Ga)Se_2$ with a critical fluence of 10^{15} ~ 10^{17} cm^{-2} depending on the energy level of incoming electrons (Garrison et al., 2018a), its effect on thermal and optical properties of ceramic materials is rarely experimentally studied, which is one of the main motivation for our study.

2 Methods

2.1 Spark plasma sintering

ZrB_2 powder from Nanografi was used. The powder has a purity of 99.5%, an average particle size of 5.5 μm, and was made of 80% zirconium and 18.9% boron in weight percent. Spark plasma sintering of zirconium diboride was performed using the FCT Systeme Gmbh SPS machine at Delft University of Technology.

Twelve cylindrical ZrB_2 samples were made in total with a diameter of 30 mm and thickness of 3 mm. Seven samples were sintered at a maximum dwelling temperature of 2000°C, and five samples were sintered at various maximum temperatures to change the densification level. The maximum sintering temperature was varied between 1800–2,000°C at increments of 50°C (1,800°C, 1,850°C, 1,900°C, 1,950°C, 2,000°C). As shown in Figure 1, the temperature was kept at the maximum for 10 min, after which it was cooled to 400°C during 64 min (25°C/min). On the other hand, the punch force was kept at 5 kN for 21 min, then held at 56 kN (~80 MPa) for 15 min and 30 s. After that, it was reduced back to 5 kN for the remaining time. About 0.2 mm of material on each side was removed after the polishing was carried out. After the samples were polished to

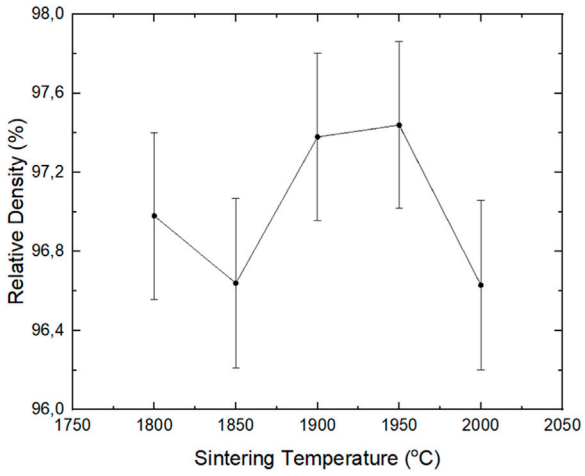

FIGURE 3
Relative densities of ZrB_2 samples sintered with increasing SPS sintering temperatures.

remove embedded graphite, they were re-polished using a standardized polishing procedure at the aerospace faculty. All the samples were cut into two-halves, one exposed to radiation and one kept unirradiated as a reference to analyze the influence of the radiation.

2.2 Radiation exposure

The electron radiation exposure was conducted using a Van de Graaf accelerator in the reaction institute at TU Delft. The electron accelerator uses a moving belt that collects charges on an insulated sphere, creating a high potential difference. The potential difference accelerates the electrons to high energies by creating an electron source. Halves of the SPS-ed ZrB_2 samples were exposed to electrons with an energy of 3 MeV at three different fluences while the other half of each pellet was kept as a reference. Electron fluences were varied by changing the irradiation time between 0 s (6 samples), 283.54 s (2 samples), 466 s (2 samples), and 1886.97 s (2 samples). This coincided with the Van de Graaf fluences and fluxes seen in Table 1. The Van de Graaf fluence was calculated assuming a 18.9, 23.0 and 28.4 μA beam current which could result in an average dose density of 59.7 kGy/cm^2 in 240 s on a Nylon material with a density of 1.15 g/cm^3.

2.3 Material characterization

The ZrB_2 samples' thermal and optical properties were measured after irradiation. Prior to the irradiation of the samples, XRD-analysis with a Rigaku Miniflex 600 and densification measurements using the Archimedes method were conducted. Thereafter, scanning electron microscopy (SEM) with a JEOL JSM7000F was conducted to investigate possible microstructural changes after irradiation at the highest fluence. Using a diamond cutter, the samples were cut into three 5 mm × 5 mm squares, then embedded into an epoxy resin with the thickness side facing up and polished. The embedded samples were thereafter sputtered in a 15 nm gold coating and had aluminum foil applied to the sides before being inserted into the SEM. Lastly, the thermo-optical properties were characterized. The coefficient of thermal expansion was measured using a PerkinElmer TMA 4000 thermo-mechanical analyzer with a temperature range of 100–600°C with a heating rate of 20 °C/min in a nitrogen flushed atmosphere. The thermal conductivity was measured using a Hot Disk TPS 2200. Room-temperature optical properties such as thermal emittance and solar absorption were measured at ESA-ESTEC in Noordwijk, the Netherlands. The thermal emittance was measured using an ET-100 handheld emissiometer measuring wavelengths between 2–3.5 μm, 3–4 μm, 4–5 μm, 5–10.5 μm and 10.5–21 μm. To measure the solar absorptance an Agilent UV-VIS-NIR spectrophotometer measured the spectra between 250–2,500 nm.

3 Results and discussion

3.1 Pre-irradiation characterization

To ensure minimal impurities were present, XRD-analysis was carried out on the purchased powder from Nanografi as well as a

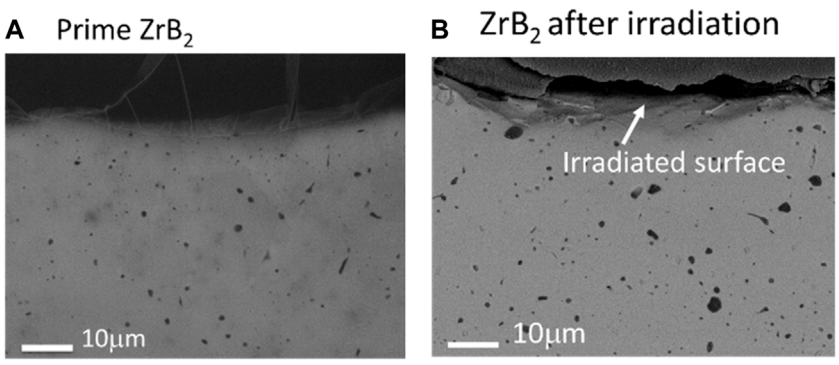

FIGURE 4
SEM images of **(A)** prime ZrB_2 and **(B)** ZrB_2 after irradiation with 3 MeV electrons for 1886.97 s. The edge (where the white arrow points) represent irradiated surface. Dark phase is hole from sintering.

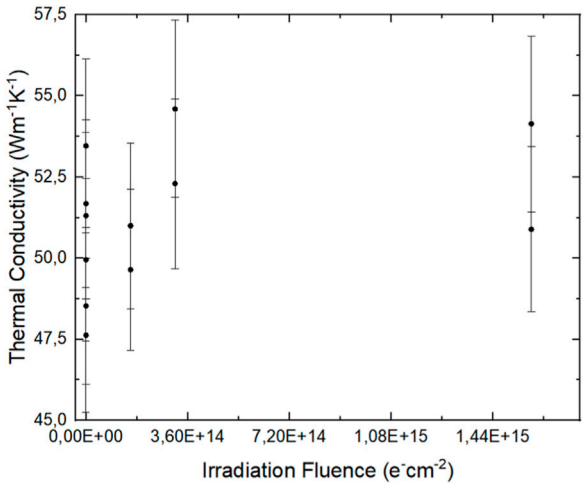

FIGURE 5
Dependence of thermal conductivity of ZrB_2 samples on the increasing irradiation fluence.

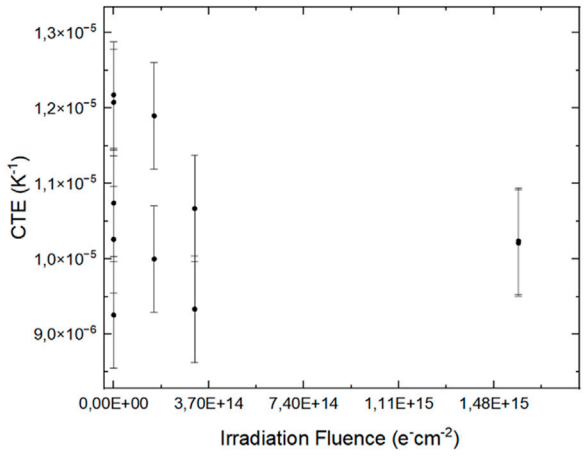

FIGURE 6
Dependence of CTE of ZrB_2 on the increasing irradiation fluence.

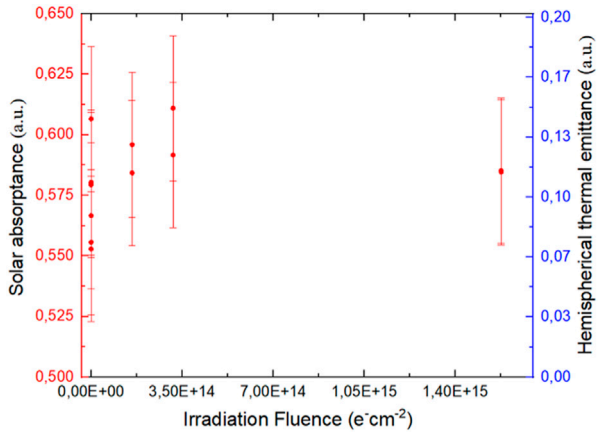

FIGURE 7
Dependence of solar absorption coefficient of ZrB_2 (left axis, red) on the increasing irradiation fluence.

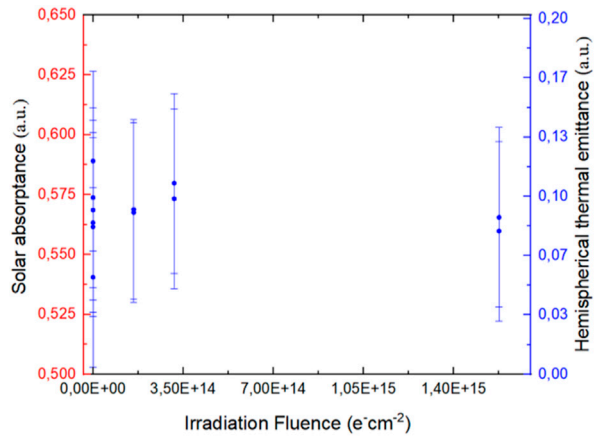

FIGURE 8
Dependence of emittance of ZrB_2 (right axis, blue) on the increasing irradiation fluence.

sintered sample (crushed into powder) prior to irradiation. By comparing these two XRD-patterns as seen in Figure 2, it can be observed that there are minimal graphite impurities (Figure 2B). Using the XRD-data, the c and a lattice parameters of the crushed samples were calculated as listed in Table 2. It can be seen that these values are close to reference values (Villars et al., 2023). The density of the ZrB_2 samples were measured to investigate the densification effect of sintering temperature. As seen in Figure 3, there was no clear correlation between sintering temperature and density, which contradicts the relationship found in literature, where as sintering temperature increases from 1800 to 1950 °C, the sintered density changes from 87% to 97% (Guo et al., 2008). A possible explanation for difference was the much higher heating rate (>200 °C/min) and shorter dwelling time (3min) at maximum temperature in the literature, which makes the effect of maximum sintering temperature more prominent. In our case, due to relatively smaller heating rate (80°C/min), an intermediate dwelling of 2 min at 1,500°C and longer dwelling time (10min) at maximum temperature, all ZrB_2 samples achieved a relative density higher than 96% in the sintering temperature range we investigated.

3.2 Irradiation effects

Figure 4 shows SEM images of the cross sections of both prime and irradiated ZrB_2 samples. It can be seen that there is no apparent microstructural degradation in the bulk. While the grains are not obvious, it can be assumed from the arrangement of the small holes (<1 μm in diameter, dark phase) that grain size remains largely unchanged after irradiation.

Figure 5 and Figure 6 display the thermal conductivity and coefficient of thermal expansion of the ZrB_2 samples plotted against increasing irradiation fluences. Despite the large

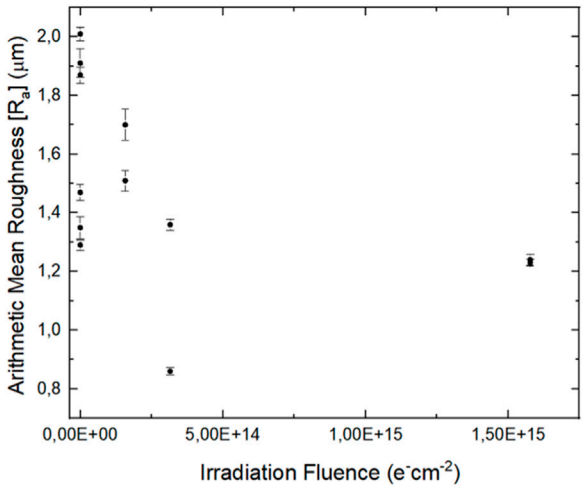

FIGURE 9
Dependence of average surface roughness of ZrB_2 samples on the increasing irradiation fluence.

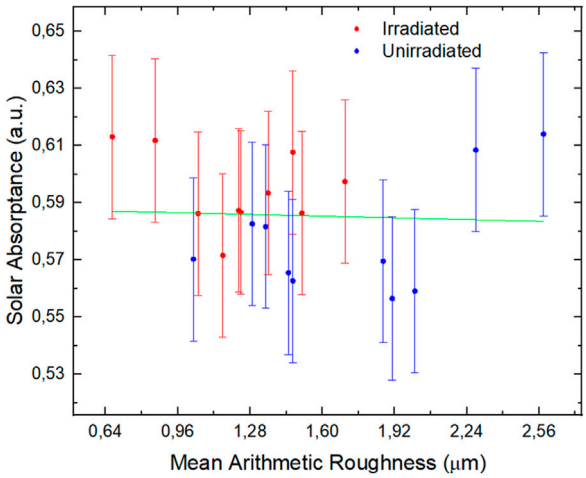

FIGURE 10
Dependence of solar absorptance on the mean arithmetic roughness of ZrB_2 samples.

uncertainties in the measurements, it can be seen that there is no obvious change. There has been quite large discrepancy in reported room temperature thermal conductivity values in literature, values as high as 88–100 Wm^{-1} K^{-1} were reported by Harrington et al. depending on the carbon content with a maximum 4.68 volume % C content (Harrington et al., 2015), while values as low as 56 W/m K was also reported by Zimmermann et al. (Zimmermann et al., 2008). A reason for this discrepancy could be contamination from balling media WC as a secondary phase in the reported literature (Zimmermann et al., 2008). Our measured thermal conductivity value (~50 W/m/K) is on the lower end as well. An investigation into the carbon content through back scattered SEM reveals the volume fraction of graphite to be less than 1%, which is in agreement with our XRD analysis (that no obvious graphite peak was detected as shown in Figure 2). This low amount of carbon is unlikely to cause such drastic reduction of thermal conductivity compared to 88 W/m/K at 4.68 volume% C in Harrington's study. While we did not use WC ball milling, we did use a different starting ZrB_2 powder which has 0.1% Si and 0.08%, 80% Zr and 18.9% B. Given the fact that additives and impurities can have a strong influence on the thermal conductivity of ZrB_2, it is not our intention to quantify what caused this low value but to seek possible change upon irradiation, which does not seem like the case.

On the other hand, our measured CTE value was ranging between 9E-6 to 1.2E-5 K^{-1}, which in fairly good agreement with reported literature values which has been measured as 6.8E-6 K^{-1} between 300 K and 1300 K whereas our measurement was done between 373 K and 873 K (Zimmermann et al., 2008). It can be seen that there is a lack of observable damage upon increasing irradiation level in the bulk thermal properties (both the thermal conductivity and CTE) of ZrB_2, which could be due to the fact that the electron irradiation level was too low. NASA has claimed that electron irradiation fluence below 10^{18} e^-cm^{-2} would not cause detectable mechanical degradation for metals, whereas for ceramic materials, large changes in the thermal

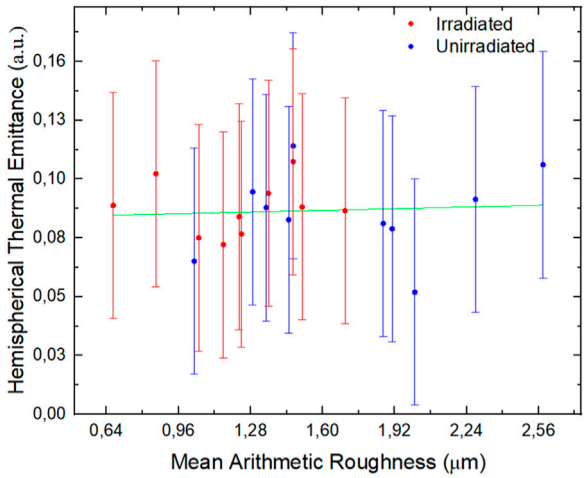

FIGURE 11
Dependence of emittance on the mean arithmetic roughness of ZrB_2 samples.

conductivity have been observed at neutron fluences of 10^{18} to 10^{19} n/cm^2 (Harold and William, 1970). However, no experimental data was provided to prove the electron radiation resistance of ceramic materials in terms of thermal properties. Albeit the fluence in the present study amounts to 10^{15} e^-cm^{-2}, it is still three orders of magnitude lower compared to the value claimed for neutrons from the NASA report, while neutrons in general cause much greater degradation compared to electrons because of heavier mass. It is speculated that if we increase the radiation time to 1,000 longer or change the radiation source to heavier particles such as proton, neutron or alpha particles, observable changes in bulk properties such as thermal conductivity and CTE may occur.

There was no significant influence on the optical properties of the increasing electron radiation fluence for the three fluences

studied as seen in Figure 7 and Figure 8. It is worth noting that the fluctuation in optical characteristics did not exceed the measurement devices' accuracy values. All the data points fell between the upper and lower uncertainty levels. It had been reported that proton irradiation on olivine, another inorganic material, generated a shift in the reflectance spectrum (Kanuchová et al., 2010) which is not observed in our case. Since there are numerous differences between the present study and that in (Kanuchová et al., 2010) (material used, irradiation particle, particle energy, particle fluence), it is difficult to pinpoint the reason why such an effect was not observed here. Moreover, a previous study also reported a color change in ZrB_2 under Helium irradiation, which would coincide with a change in absorption properties in the visual spectrum range (Garrison et al., 2018b). In this case, the irradiation energy was 30 keV, but the radiation fluence was significantly higher with values such as 8.4×10^{21} He/m^2 and 5×10^{22} He/m^2. The main difference between study (Garrison et al., 2018b) and the present study was the use of heavier ion irradiation at higher fluences instead of electron irradiation, which causes significantly more damage to the material. Therefore, the absence of ion implantation and ion sputtering could be contributing factors as to why there was no damage to the optical properties by electron irradiation. Additionally, the electrons have a larger penetration depth so could have caused damage deeper in the ZrB_2 samples and consequently limited damage on the surface.

Figure 9 displays the R_a of the irradiated samples against the irradiation fluence. This is only plotted for samples produced at the same sintering temperature of 2000°C. No apparent influence on R_a can be observed from the three irradiation fluences tested. Similarly, to the thermal property measurements, within the same irradiation fluence (see 3.15E14 e$^-$/cm^2), there was a more significant change in Ra than with increasing fluence. There was limited research which investigated the influence of irradiation on the surface roughness of materials, and none with ZrB_2. In the study by Carter and Vishnyakov, it was found that silicon had a significantly lower surface roughness under normal incidence Xe^+-ion irradiation compared to irradiation with incidence angles between 0–40° (Carter and Vishnyakov, 1996). Although surface roughness values were lower for irradiated samples in the present study, it is yet to be further investigated if this is indeed caused by irradiation such as electron sputtering, or rather an artifact of polishing. More intense irradiation would have caused larger-scale damage to the surface of ZrB_2, which should have been visible in SEM imaging after irradiation and thus help clarify this question.

3.3 Surface roughness and optical properties

Figure 10 displays the absorptance and R_a for all the measured samples sintered from different temperatures. Based on the linear fit, there was a weak negative correlation between the two variables, albeit with a meager r-squared value. A similar case was seen with the hemispherical thermal emittance measurements in Figure 11, where a weak positive correlation was observed.

According to Wen et al. (Wen and Mudawar, 2006), there exists a relationship between the surface roughness, resistivity and infrared emissivity of thin films, which can be explained by the following mathematical models,

$$R_r = R_p \exp\left[\left(-\frac{4\pi\sigma}{\lambda}\right)^2\right]$$

Where Rr and Rp represent the reflectance of a rough and smooth surface, respectively, σ corresponds to the root-mean-square roughness and λ refers to the wavelength. According to this theoretical model, higher surface roughness will lead to lower reflectance and thus higher emissivity at a specific wavelength. Zhang et al. (Zhang et al., 2020) discovered that when the surface roughness of ZrB_2 films was in nanometer-scale, it did not show a remarkable effect on the infrared emissivity of ZrB_2 thin films. In our study, the surface roughness is in the micrometer range (0.6–2.6 μm), and we observed a weak dependence, as shown in Figure 10 and Figure 11. It is reasonable for us to conjure if the roughness range were enlarged, greater optical property change would potentially be observed.

What we can conclude also, is that the irradiated samples generally had a lower mean arithmetic roughness than the unirradiated samples. This could indicate a smoothing surface effect from the irradiation originating from effects such as electron sputtering.

4 Conclusion

In this study we have looked into the electron irradiation resistance of thermal and optical properties of ZrB_2 for thermal protection systems. Although further investigation remains to be carried on to bring to full conclusion, what we can conclude so far based on this study are: 1) varying the sintering temperature did not influence the radiation resistance of ZrB_2's thermo-optical properties due to a lack of positive correlation between sintered density and sintering temperature. Our sintering parameters (two-stage sintering, slow heating rate, long dwell time at maximum temperature) will yield a consistent sintering density 97+/−0.6%; 2) current irradiation fluence (10^{15} e$^-$cm^{-2}) is not large enough to cause drastic change in thermal conductivity and thermal expansion coefficient, namely, no obvious bulk property changes. An irradiation time at least 1,000 larger is proposed to cause severe observable bulk damage, otherwise heavier irradiation sources are needed. 3) While no obvious optical property change was observed based on irradiation fluence change, a weak dependence between optical properties and surface roughness was observed. Given the critical influence of optical properties for thermal protection system application, we propose surface roughness as a potential tunable parameter for future thermal design.

It can be concluded that the electron radiation had no significant influence on the thermo-optical characteristics of ZrB_2 and the material showed to be highly electron irradiation resistant in the irradiation fluences investigated (up to E15 e$^-$/cm^2). In view of its use as a thermal protection system in spacecraft, these are promising results, implying thermos-optical stability within the investigated parameter range. However, longer irradiation duration and consequently larger fluence would be beneficial to probe into

longer term use of ZrB_2. Moreover, a detailed irradiation dose analysis in Van Allen belt, which would likely impose higher radiation dose, is needed to properly conclude the irradiation resistance of ZrB_2 for long-term use in high earth orbits such as geostationary orbit Weinert et al., 2003.

Data availability statement

The original contributions presented in the study are included in the article/Supplementary material, further inquiries can be directed to the corresponding author.

Author contributions

DR: Data curation, Formal Analysis, Investigation, Methodology, Writing–original draft, Writing–review and editing. YT: Conceptualization, Funding acquisition, Methodology, Project administration, Resources, Supervision, Validation, Writing–review and editing.

Funding

The author(s) declare that financial support was received for the research, authorship, and/or publication of this article. This work was supported by the master thesis program from aerospace structures and materials department in the aerospace engineering faculty in TU Delft, Netherlands.

Acknowledgments

The authors would like to acknowledge Hans Brouwer, Roy Awater, Nuno Dias, Lennart van Den Hengel and Yun-Ching Lin for their valuable input and assistance during the project.

Conflict of interest

The authors declare that the research was conducted in the absence of any commercial or financial relationships that could be construed as a potential conflict of interest.

Publisher's note

References

Carter, G., and Vishnyakov, V. (1996). Roughening and ripple instabilities on ion-bombarded Si. *Phys. Rev. B* 54, 17647–17653. doi:10.1103/PhysRevB.54.17647

Christa, B.-K., and Facius, R. (2002). "Life under conditions of ionizing radiation," in *Astrobiology* (Berlin, Germany: Springer), 261–284. ISBN: 3-540-42101-7. doi:10.1007/978-3-642-59381-9_18

EPA (2020). Effects of radiation damage. Available at: https://www.epa.gov/radiation/radiation-health-effects.

Garrison, L. M., Kulcinski, G. L., Hilmas, G., Fahrenholtz, W., and Meyer, H. M. (2018a). The response of ZrB2 to simulated plasma-facing material conditions of he irradiation at high temperature. *J. Nucl. Mater.* 507, 112–125. ISSN: 0022-3115. doi:10.1016/j.jnucmat.2018.04.016

Garrison, L. M., Kulcinski, G. L., Hilmas, G., Fahrenholtz, W., and Meyer, H. M. (2018b). The response of ZrB2 to simulated plasma-facing material conditions of He irradiation at high temperature. *J. Nucl. Mater.* 507, 112–125. ISSN: 0022-3115. doi:10.1016/j.jnucmat.2018.04.016

Guo, S.-Q., Nishimura, T., Kagawa, Y., and Yang, J. (2008). Spark plasma sintering of zirconium diborides. *J. Am. Ceram. Soc.* 91 (9), 2848–2855. doi:10.1111/j.1551-2916.2008.02587.x

Guria, J. F., Bansal, A., and Kumar, V. (2021). Effect of additives on the thermal conductivity of zirconium diboride based composites – a review. *J. Eur. Ceram. Soc.* 41 (1), 1–23. ISSN:0955-2219. doi:10.1016/j.jeurceramsoc.2020.08.051

Harold, S., and William, S. G. (1970). "Nuclear and space radiation effects on materials," in *NASA space vehicle design criteria (Structures)* (Washington, D.C., United States: NASA).

Harrington, G. J. K., Hilmas, G. E., and Fahrenholtz, W. G. (2015). Effect of carbon on the thermal and electrical transport properties of zirconium diboride. *J. Eur. Ceram. Soc.* 35, 887–896. doi:10.1016/j.jeurceramsoc.2014.09.035

Johnson, S. M., Johnson, S. M., Squire, T. H., Lawson, J. W., Gusman, M., Lau, K. H., et al. (2014). "Biologically-derived photonic materials for thermal protection systems," in Annual Conference on Composites, Materials, and Structures, Cocoa Beach, FL, United States, January, 2014.

Kanuchová, Z., Baratta, G. A., Garozzo, M., and Strazzulla, G. (2010). Space weathering of asteroidal surfaces* - influence on the UV-Vis spectra. *Astronomy Astrophysics* 517, A60. doi:10.1051/0004-6361/201014061

Sengupta, P., and Manna., I. (2019). Advanced high-temperature structural materials for aerospace and power sectors: a critical review. *Trans. Indian Inst. Met.* 72, 2043–2059. doi:10.1007/s12666-019-01598-z

Villars, P., and Cenzual, K. (2023). *ZrB2 crystal structure*. Berlin, Germany: Springer-Verlag.

Weinert, K., Jasenek, A., and Rau, U. (2003). Consequence of 3-MeV electron irradiation on the photovoltaic output parameters of Cu(In,Ga)Se2 solar cells. *Thin Solid Films* 431–432, 453–456. doi:10.1016/S0040-6090(03)00181-0

Weisensee, P. B., Feser, J. P., and Cahill, D. G. (2013). Effect of ion irradiation on the thermal conductivity of UO2 and U3O8 epitaxial layers. *J. Nucl. Mater.* 443 (1), 212–217. ISSN:0022-3115. doi:10.1016/j.jnucmat.2013.07021

Wen, C.-D., and Mudawar, I. (2006). Modeling the effects of surface roughness on the emissivity of aluminum alloys. *Int. J. Heat. Mass Transf.* 49, 4279–4289. doi:10.1016/j.ijheatmasstransfer.2006.04.037

Zhang, M., Ma, X., Yin, J., Zhang, Y., Zhang, L., Zhou, Y., et al. (2020). Experimental and theoretical modeling study on the infrared properties of ZrB2 thin film. *Thin Solid Films* 709, 138140. doi:10.1016/j.tsf.2020.138140

Zimmermann, J., Hilmas, G., Fahrenholtz, W., Dinwiddie, R., Porter, W., and Wang, H. (2008). Thermophysical properties of ZrB2 and ZrB2–SiC ceramics. *J. Am. Ceram. Soc.* 91, 1405–1411. doi:10.1111/j.1551-2916.2008.02268.x